Photovoltage dynamics of the hydroxylated Si(111) surface investigated by ultrafast electron diffraction

Ryan A. Murdick, Ramani K. Raman, Yoshie Murooka, and Chong-Yu Ruan*

Department of Physics and Astronomy, Michigan State University, East Lansing, Michigan 48824-2320, USA

We present a method to measure transient photovoltage at nanointerfaces using ultrafast electron diffraction. In particular, we report our results on the photoexcitation of carriers and their ensuing relaxations in a hydroxyl-terminated silicon surface, which is a standard substrate for fabricating molecular electronics interfaces. The transient surface voltage is determined by observing Coulomb refraction changes induced by the modified space-charge barrier within a selectively probed volume by femtosecond electron pulses. The results are in agreement with ultrafast photoemission studies of surface-state charging, suggesting a surface charge relaxation mechanism closely coupled to the bulk carrier dynamics near the surface that can be described by a drift-diffusion model. This study demonstrates an ultrafast diffraction method for investigating interfacial processes with both charge and structural resolutions.

I. INTRODUCTION

The problem of directly converting solar energy into electrical energy through photocarrier generation has recently gained tremendous attention due to new types of photovoltaic (PV) cells utilizing nanoparticles and molecular interfaces.[1–5] An important parameter determining the efficiency of the solar cell is the survival rate of photogenerated carriers reaching the electrodes, which is strongly affected by surface recombination and the transport characteristics at the contacts. In a Schottky-type PV junction, the carrier dynamics are driven by a space-charge barrier layer.[6] A photovoltage is generated as the photoinduced electron-hole pairs near the semiconductor interface move to reduce the band bending. More generally, diffusion of nonequilibrium carriers,[7–9] charging of the surface states,[10] and photoionization[11] are different contributors for emfs at semiconductor junctions, attributing to the overall magnitude and sign of the generated photovoltage. For a molecular interface, the existence of discrete surface and/or charge-transfer states are crucial in directing the carrier separation in new generation PV cells such as dye-sensitized TiO$_2$ mesoporous films[2] and quantum dot solar cells.[3,5] In these cases, the filling of a surface state can strongly affect the charge distribution in the space-charge layer, modifying the transport characteristics as revealed in photoemission studies.[10,12,13] Surface charging is also essential for explaining surface photochemical processes including catalysis[14] and molecular transport.[15] Here, we use a diffractive potentiometry approach to determine the transient photovoltage based on the ultrafast electron diffraction technique whose ability to resolve surface structure evolution has been demonstrated previously.[16,17]

We study the photoinduced surface-potential changes on a Si(111) surface terminated with hydrophilic hydroxyl (OH) groups, a prototypical system for fabricating molecular electronic devices.[18,19] The experiment is performed in an optical pump-diffraction probe arrangement in which the femtosecond laser pulse is used to initiate carrier generation near the surface and in turn, the formation of a transient surface voltage (TSV), while a charge-sensitive electron pulse probes the ensuing carrier relaxation dynamics. A Coulomb refraction formalism is deduced to treat ultrafast diffraction data to determine the TSV. Using a laser fluence (F) of 22 mJ/cm^2, we found a band-flattening TSV of 300 mV generated 30 ps after the laser excitation. At higher fluences (F > 72 mJ/cm^2), the TSV continued to rise even beyond the band gap energy. This surprisingly large TSV is attributed to a modified barrier due to a nonequilibrium surface charge migration induced by photoexcitation.[13] We observed picosecond charge injection and relaxation dynamics with timescales similar to results obtained using ultrafast photoemission studies of surface carrier dynamics in a vacuum cleaved Si(111)−(2×1) surface.[10] This rapid recovery can be understood based on a drift-diffusion model that couples surface carrier dynamics with transport in the space-charge layer. This suggests that the hydroxylated silicon interface is highly rechargeable with long-lived trap states ideal for mediating molecular electronic transport study.[19]

II. EXPERIMENT DETAILS

A. Sample preparation

The hydroxylated Si(111) surface was prepared *ex situ* using a wet chemistry method. The as-received Si(111) wafer (Silicon Quest Intl., *p* type, roughness < 12 μm) was treated with a modified RCA procedure.[20] The native oxide layer, which usually contains a high density of trap states, was removed and an ultrathin (< 5 nm) oxidation layer with high electric quality was grown. First, the wafer was immersed in H$_2$SO$_4$/H$_2$O$_2$ (7:3) solution at 90 °C for 10 min to remove surface contaminants. The surface was then etched with a 40% NH$_4$F solution[21] to remove the native oxide layer followed by a bath in NH$_4$OH/H$_2$O$_2$/H$_2$O (1:1:5) at 80 °C for 20 min to further remove inorganic residues. A hydroxylated surface was grown on a thin layer of oxide by immersing the wafer in HCl/H$_2$O$_2$H$_2$O/ (1:1:6) at 80 °C for 10 min. The wafer was rinsed with de-ionized water (17.8 MΩ cm) for 10 min at the end of each cycle. This procedure yields a density of ≈10^{15} cm^{-2} silanol groups (Si-OH) on the surface.[19]
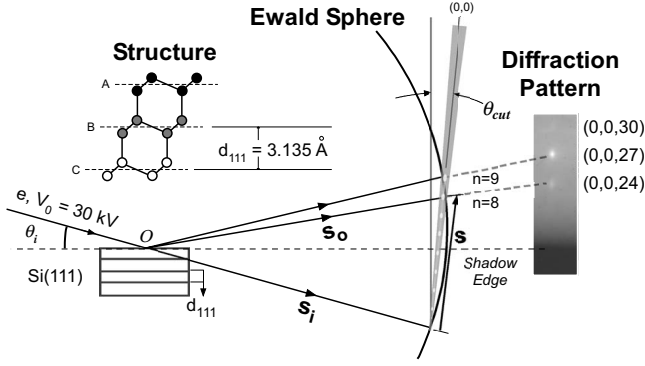
FIG. 1. Electron scattering geometry. The incident beam s_i (energy eV_0, incidence angle θ_i, and Ewald sphere origin O) scatters off the Si(111). Constructive interference occurs when the scattered beam (s_o) crosses an intersection of the Ewald sphere with a reciprocal-lattice rod. Here, surface steps from Si(111) cleave tilt the reciprocal lattice rods by θ_{cut}, resulting in interference maxima below the projected zeroth-order Laue zone. From the observable peaks (0,0,24), (0,0,27), and (0,0,30), we measured $\Delta s = 1.985$ Å^{-1}, implying interlayer spacing of $d_{111} = 2\pi/\Delta s = 3.165$ Å and $\theta_{cut} \approx 1.35°$. The ABC stacking of Si(111) diamond lattice has lattice constant 9.406 Å, implying an interlayer spacing of $d_{111} = 3.135$ Å in agreement with our measurements.

B. Transient surface potential determined by ultrafast electron diffraction

The experiment was conducted in the ultrafast electron crystallography setup,[17] employing the reflection geometry to gain surface sensitivity. As described in Fig. 1, the incident probe electron has a kinetic energy $K_0 = eV_0$, where $V_0 = 30$ kV is the accelerating voltage corresponding to an incident reciprocal wave vector $s_i = 90$ Å^{-1}. At an incidence angle $\theta_i = 6.8°$ the Ewald sphere intersects the (0,0) reciprocal lattice rod of the Si(111) substrate near momentum-transfer wave vector $s \approx 18$ Å^{-1}, producing an in-phase (0,0,27) diffraction maximum on the screen. Since the Si(111) substrate has a slight miscut ($\theta_{cut} \approx 1.35°$), the diffraction maxima appear slightly below the projected zeroth-order Laue zone. Weak (0,0,24) and (0,0,30) (Ref. 22) diffraction maxima arising from the surface roughness were also observed. These maxima are associated with the interference pattern of Si(111) planes evident from $\Delta s = 1.985$ Å^{-1} between neighboring peaks satisfying the reciprocal relationship $d_{111} = 2\pi/\Delta s$ with an accepted d_{111} value of 3.135 Å. The electron penetration depth in silicon is estimated to be ≈ 2 nm based on the Scherrer criterion[23] using the width of the (0, 0, 27) diffraction maximum.

To determine the surface potential, we examine the Coulomb refraction introduced by a surface potential for electron diffraction as shown in Fig. 2(a). The surface potential V_s alters the kinetic energy of the electrons submerged in the crystal, $K' = e(V_0 + V_s)$, without changing the transverse momentum, thereby causing a refraction at the interface. The index of refraction can be described by $n_e = \sqrt{(V_s + V_0)/V_0}$ (Ref. 24). For surface diffraction, this alters the electron incidence angle toward the lattice plane, thus introducing a net
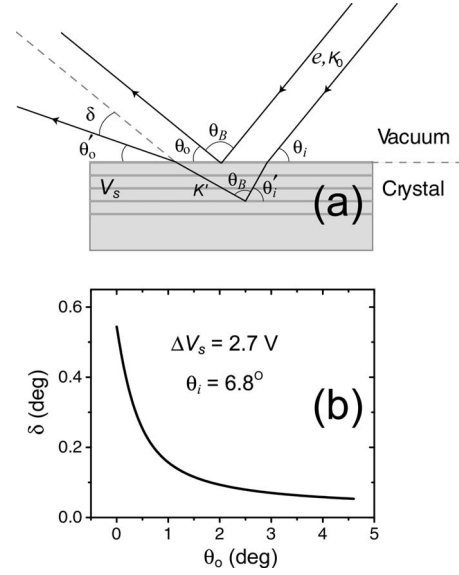

FIG. 2. (a) Ray traces of the electron path with and without a surface potential (V_s) present. V_s induces a shift δ in the diffraction maxima. (b) The shift in diffraction peak maxima as a function of θ_o. Lower order diffraction maxima shift more than higher orders in the presence of a surface potential.

angular shift (δ) of the diffraction maximum. We calculate the shift arising from a surface potential to be

$$\frac{V_s}{V_0} = \frac{(\theta_o \delta - \theta_i \theta_o + \delta^2/2)^2 - \theta_i^2 (\theta_o + \delta)^2}{(\theta_i + \theta_o)^2}, \quad (1)$$

where all symbols are defined in Fig. 2(a). In the optical pump-diffraction probe experiment, V_s is replaced by the transient surface voltage ΔV_s to evaluate the photoinduced refraction shift of diffraction maxima at θ_o. The dependence of δ on θ_o is shown in Fig. 2(b) and calculated using Eq. (1) with our incidence angle ($\theta_i = 6.8°$) and $\Delta V_s = 2.7$ V. This refraction shift has a "nonstructural" characteristic exhibiting a more significant deviation at smaller values of θ_o. This differs fundamentally from structure-induced shifts, which behave oppositely. For small-angle diffraction the Bragg law yields a monotonic increase in δ as a function of θ_o for a given structural change Δd as described by $\delta/(\theta_o + \theta_i) = \Delta d/d$, i.e., the higher-order diffraction maxima experience proportionally larger shifts than the lower-order ones. This clear distinction allows us to separate Coulomb-induced effects from structural changes by analyzing multiple diffraction maxima. To demonstrate the principle, we will follow both (0,0,24) and (0,0,27) diffraction maxima to examine the TSV dynamics.

III. RESULTS

The characteristic features associated with the Coulomb effect were observed experimentally as shown in Fig. 3(a). Using a laser fluence of 72 mJ/cm^2, the time-dependent shifts of diffraction maxima (0,0,24) and (0,0,27) were followed by adjusting the arrival time of the electron probe pulse relative to that of the exciting laser pulse. The shift of
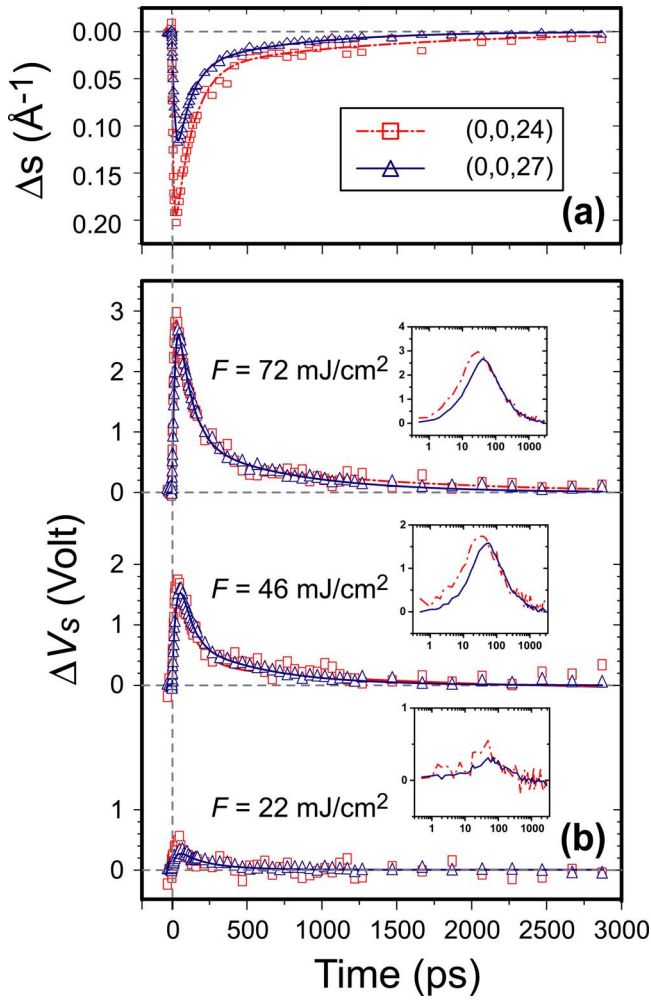
FIG. 3. (Color online) (a) Transient shift in diffraction maxima induced by the TSV. The shift in peak (0,0,24) nearly doubles that of (0,0,27), indicating the presence of a TSV. (b) The TSV for the laser fluences employed. Insets: semilog TSV, demonstrating the contrasting behavior in the TSV rise for the given peaks.

the (0,0,24) diffraction maximum in reciprocal space is markedly greater than that associated with (0,0,27), pointing to a Coulomb effect. We expect a negligible structure-induced shift because of the small absorption coefficient in silicon ($\alpha^{-1} \approx 1$ μm) for the near infrared excitation ($h\nu = 155$ eV), indicating that the thermal energy deposition is spread out over a large volume. The maximum temperature rise in Si can be estimated from $\Delta T_L = C_L^{-1}\alpha F(1-R)(h\nu - E_g)/h\nu + C_L^{-1}\Delta n_{e-h}E_g$, where $R = 0.37$ is the reflectivity, $C_L = 2.08 \times 10^6$ Jm^{-3} K^{-1} is the lattice heat capacity, and Δn_{e-h} is the carrier density drop due to Auger recombination.[25] The laser fluences we applied ranged from 22 to 72 mJ/cm^2, which give rise to only moderate increases in lattice temperature from approximately 20 to 170 K, respectively, above the initial temperature $T_0 = 300$ K. Hence the changes induced by lattice heating $\Delta s/s$ are on the order of 10^{-4} based on the thermal expansion coefficient for Si (Ref. [26]). In contrast, the carrier generation is more significant, ranging from 5×10^{20} to 1.4×10^{21} cm^{-3}, which corresponds to an increase in several orders of magnitude from the intrinsic carrier con-

centration ($10^{15}-10^{16}$ cm^{-3}) within the first picosecond.[25] Since we have observed changes on the order of 10^{-2}, we expect that the lattice heating has negligible effect in deriving the TSV from our data. By applying Eq. (1), where $\delta = \sin^{-1}(\Delta s/s_i)$ and $\theta_o = \sin^{-1}(s/s_i)$, we are able to determine the TSV for both (0, 0, 24) and (0, 0, 27) for $F = 22, 46$, and 72 mJ/cm^2. The TSVs thus derived are self-consistent for both Bragg maxima with the maximum change ranges from 0.3 to 3 V shown in Fig. 3(b), demonstrating the robustness of the diffractive TSV measurement. With the induced 4–5 orders of magnitude increase in carrier concentration, it is expected that the equilibrium surface band bending, which is ≈ 0.3 V (Ref. [27]) will be flattened out easily. Indeed, this is the case at the lowest fluence applied ($F = 22$ mJ/cm^2), where a TSV of 0.38 V was determined. However, TSVs higher than the initial band bending were also observed; 1.74 and 2.97 V for fluences of 46 and 72 mJ/cm^2, respectively. Such large TSVs at early times represent a new regime where the nonequilibrium carrier dynamics caused by femtosecond laser initiation must be considered.

As mentioned, the significant photovoltage induced by the high-fluence femtosecond laser cannot be explained merely by a barrier-layer effect where photoinduced *e-h* pairs near the semiconductor interface separate to screen the surface charges responsible for the band bending. Without modifying surface charge population, this theory would predict a maximum TSV corresponding to the dark current band bending[28] and the decay time of the TSV would be comparable to the characteristic bulk recombination time ($\approx 10-100$ ns for Si). In contrast, we have witnessed a much more rapid process with the TSV surging within 30 ps following laser excitation and a decay on the order of 100 ps for each of the three different fluences without any saturation as shown in Fig. 3(b). Enhanced surface band bending was also observed by Marsi *et al.*[13] in studying the transient charge distribution at the SiO$_2$/Si interface following UV free-electron laser excitation using time-resolved pump-probe core photoemission spectroscopy. The cause of the enhancement is attributed to electron diffusion into the thermally grown SiO$_2$ overlayer and subsequent accumulation at its surface. The recombination of the excess electrons was found to be slower with thicker oxide layers. For 12 Å oxide thickness, the surface charge recombination was found to be comparable to the typical excess carrier recombination time in the Si(111) space-charge layer of the order of 100 ns. For very thin (a few angstrom) oxide layers, a very effective "surface" recombination process was observed within their time resolution of ≈ 200 ps. These observations are consistent with a picture in which the surface recombination rate is determined by the separation between the excess surface electrons and excess holes in the Si space-charge layer. Indeed, much shorter recombination time is found for the decay of the surface-state population in a vacuum-cleaved Si surface.[10] This speedup in surface recombination for an ultrathin oxide layer (<1 nm) observed by Marsi *et al.* is attributed to the enhanced overlap of bulk evanescent states of Si with the surface states. In that case and in the studies reported here, the electrons accumulated at the thin oxide surface are so close to the Si space-charge layer that their role in the recombination process is similar to the normal surface state.
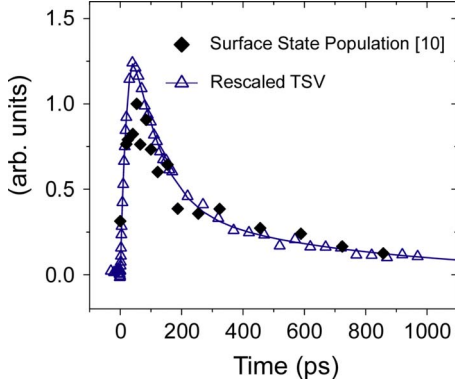
FIG. 4. (Color online) Transient surface-state population measured by photoemission (Ref. 10) compared to the measured TSV (rescaled; $F=72$ mJ/cm^2), demonstrating very similar decay rates.

The decay behavior of the TSV on the hydroxylated Si(111) surface was compared with the surface-state dynamics on a vacuum-cleaved Si(111)−(2×1) surface revealed by a photoemission study (Fig. 4).[10] In this figure, the TSV is rescaled to match with the data extracted from Ref. 10. We find a striking similarity between the two, suggesting that the surface-state population is in quasiequilibrium with the bulk carrier dynamics in the space-charge layer, so long as there is strong coupling between the surface state and the bulk evanescent state. Further evidence of the strong role played by carrier dynamics on the surface recombination is revealed by the power-law decay of the TSV shown in Fig. 5(a) where an exponent near −1 (−0.93 ± 0.03) is ascribed to the characteristic decay of surface charges with a time constant of 100 ps.

IV. DISCUSSION AND CONCLUSIONS

To describe the population decay of the surface state driven by a space-charge drift recombination, we introduce a simple two-slab model illustrated in Fig. 5(b)–5(d). The electrons accumulated at the surface lead to a rapid rise in surface potential within the thin oxide layer that decays slowly into the Si space-charge region as depicted in Fig. 5(b). The nonequilibrium space-charge layers with an initial separated charge density σ_0 are modeled as two separate slabs separated by a distance l_{e-h} in a dielectric medium ($\epsilon \approx 13$ for Si) shown in Fig. 5(c). The power-law characteristics are manifested in the simple rate equation $d\sigma(t)/dt = \sigma(t)/\tau_r$ with the space-charge recombination time $\tau_r = l_{e-h}/\mu E$ depending on the transient field E, which is directly related to the surface charge $\sigma(t)$. Its solution $\sigma(t) = \sigma_0/(t/\tau_c + 1)$ has a characteristic timescale $\tau_c = l_{e-h}\epsilon/\mu\sigma_0$, which is the time for the TSV to drop by 50% from its initial value and corresponds to the induction period in the log-log plot of the solution as described in Fig. 5(d). For $t \gg \tau_c$, the t^{-1} behavior emerges similar to what is observed experimentally [Fig. 5(a)]. To compare with the experimental results, we assume a linear decay of the surface-potential barrier (V_s) over the space-charge layer l_{e-h} and determine the size of the induced space-charge regime to be $l_{e-h} \approx 400$ nm (using carrier mobility, $\mu = 100$ cm^2 V^{-1} s^{-1} according to Ref. 25, our measured τ_c of
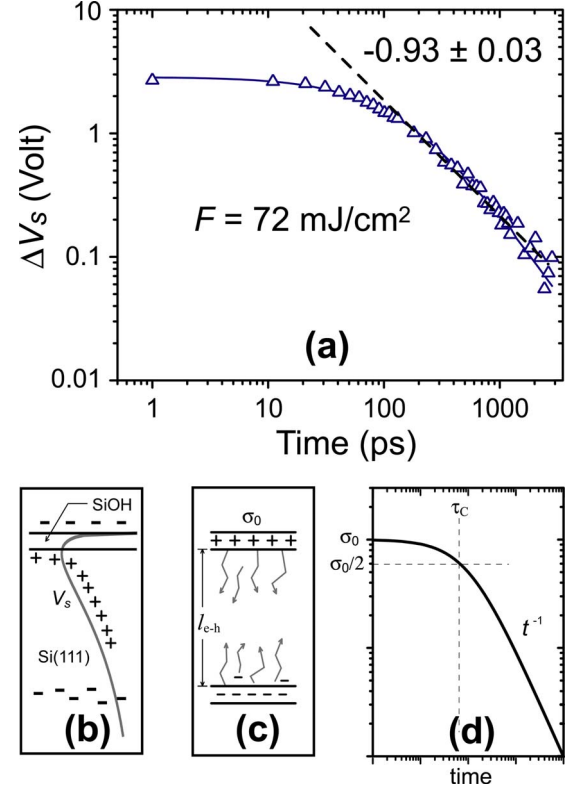

FIG. 5. (Color online) (a) Log-log plot of the TSV. (b) Surface potential (V_s) at the SiOH/Si(111) interface depicted by solid gray line. (c) Two-slab model employed (schematic) to describe the space-charge region. (d) Carrier drift causes the surface charge (σ_0) to diminish with characteristic time τ_c; after which, σ_0 falls as t^{-1} obtained from the two-slab model.

100 ps, and V_s of 2 V), which is in agreement with the laser penetration depth in Si.

Other mechanisms that would also affect the TSV decay include the ambipolar diffusion of the bulk excess carriers away from the surface and the decay of the surface-state charges into trap states. Here, we can exclude ambipolar diffusion as the main cause of TSV decay for two reasons. First, the characteristic diffusion time τ_{diff} is significantly longer than what we observed ($\tau_{diff} = l_{e-h}^2/D_{e-h} \approx 700$ ps, based on the excess e-h region generated by the laser, $l_{e-h} \approx 1$ μm, and ambipolar diffusivity $D_{e-h} \approx 15$ cm^2 s^{-1}) (Ref. 25). Second, a $t^{-1/2}$ decay is expected in the case of one-dimensional diffusion,[29] which is appropriate for photoexcitation when the laser spot size (600 μm) is large compared to the penetration depth (≈ 1 μm). The rapid decay of the TSV after 100 ps precludes any long-lived trap state from playing a significant role. Halas and Bokor[10] invoked coupled drift-diffusion Poisson equations for bulk carriers to self-consistently treat the surface-state dynamics. Such calculation is able to describe the general behavior of the surface-state depopulation and TSV decay (to be reported elsewhere[30]). However, the essential power-law behavior can be elucidated with a simple space-charge recombination model as described above.

While the simple Coulomb refraction formalism described in Eq. (1) seems to be adequate for deducing consistent

TSVs from diffraction maxima especially for the recombination dynamics, some departure between the TSVs deduced for (0,0,24) and (0,0,27) is evident at short times as depicted in the insets of Fig. 3(b). This discrepancy is believed to be caused by a nonequilibrium barrier layer, which deviates significantly from a homogeneous potential model assumed in Eq. (1) within the electron probed volume. More rigorous treatment of the Coulomb refraction formalism with a non-homogeneous potential is needed to fully account for the short-time dynamics.

In conclusion, we have demonstrated a method of directly measuring transient surface potential using ultrafast electron diffraction. In comparison to the other commonly used surface imaging techniques such as Kelvin force and scanning tunneling microscopy, we are able to examine surface-potential changes from the femtosecond to nanosecond timescales. This technique is complementary to ultrafast photoemission methods in which the energetics of the photoemitted electrons (rather than the potential) are directly measured. Since our employed electron probe energy is reasonably high, it allows surface-potential characterization at high laser excitation fluences, which are usually inaccessible by the low energy photoemission techniques due to the space-charge effect.[31] We have revealed a regime of strong photoinduced surface voltage rise, which can serve as an impulsive current source for investigating time-dependent transport at nanointerfaces.

*ruan@pa.msu.edu

[1] W. U. Huynh, X. G. Peng, and A. P. Alivisatos, Adv. Math. **11**, 923 (1999).

[2] M. Gratzel, Nature (London) **414**, 338 (2001).

[3] A. J. Nozik, Physica E (Amsterdam) **14**, 115 (2002).

[4] M. D. Kelzenberg, D. B. Turner-Evans, B. M. Kayes, M. A. Filler, M. C. Putnam, N. S. Lewis, and H. A. Atwater, Nano Lett. **8**, 710 (2008).

[5] K. S. Leschkies, R. Divakar, J. Basu, E. Enache-Pommer, J. E. Boercker, C. B. Carter, U. R. Kortshagen, D. J. Norris, and E. S. Aydil, Nano Lett. **7**, 1793 (2007).

[6] W. Schottky, Phys. Z. **31**, 913 (1930).

[7] L. D. Landau and E. Lifshitz, Phys. Z. Sowjetunion **9**, 477 (1936).

[8] N. F. Mott, Proc. R. Soc. London, Ser. A **171**, 281 (1939).

[9] J. Tauc, Rev. Mod. Phys. **29**, 308 (1957).

[10] N. J. Halas and J. Bokor, Phys. Rev. Lett. **62**, 1679 (1989).

[11] J. E. Demuth, W. J. Thompson, N. J. DiNardo, and R. Imbihl, Phys. Rev. Lett. **56**, 1408 (1986).

[12] J. P. Long, H. R. Sadeghi, J. C. Rife, and M. N. Kabler, Phys. Rev. Lett. **64**, 1158 (1990).

[13] M. Marsi *et al.*, Phys. Rev. B **61**, R5070 (2000).

[14] B. Yoon, H. Hakkinen, U. Landman, A. S. Worz, J. M. Antonietti, S. Abbet, K. Judai, and U. Heiz, Science **307**, 403 (2005).

[15] G. C. Liang, A. W. Ghosh, M. Paulsson, and S. Datta, Phys. Rev. B **69**, 115302 (2004).

[16] A. H. Zewail, Annu. Rev. Phys. Chem. **57**, 65 (2006).

[17] C.-Y. Ruan, Y. Murooka, R. K. Raman, and R. A. Murdick, Nano Lett. **7**, 1290 (2007).

[18] A. N. Shipway, E. Katz, and I. Willner, ChemPhysChem **1**, 18 (2000).

[19] D. K. Aswal, S. Lenfant, J. V. Guerin, D. Yakhmi, and D. Vuillaume, Anal. Chim. Acta **568**, 84 (2006).

[20] W. Kern and D. A. Puotinen, RCA Rev. **31**, 187 (1970).

[21] G. S. Higashi, R. S. Becker, Y. J. Chabal, and A. J. Becker, Appl. Phys. Lett. **58**, 1656 (1991).

[22] The signal-to-noise ratio for this peak was too weak to follow dynamically.

[23] A. L. Patterson, Phys. Rev. **56**, 978 (1939).

[24] Z. L. Wang, *Reflection Electron Microscopy and Spectroscopy for Surface Analysis* (Cambridge University Press, New York, 1996).

[25] J. K. Chen, D. Y. Tzou, and J. E. Beraun, Int. J. Heat Mass Transfer **48**, 501 (2005).

[26] V. M. Glazov and A. S. Pashinkin, High Temp. **39**, 413 (2001).

[27] W. Widdra *et al.*, Surf. Sci. **543**, 87 (2003).

[28] L. Kronik and Y. Shapira, Surf. Sci. Rep. **37**, 1 (1999).

[29] D.-S. Yang, N. Gedik, and A. H. Zewail, J. Phys. Chem. C **111**, 4889 (2007).

[30] R. A. Murdick, C.-Y. Ruan, and R. E. Mickens (unpublished). Electron and hole motions are described by the drift-diffusion Poisson (DDP) coupled partial differential equations. We integrate the field from the DDP system over our probe depth, allowing us to compare the numerically calculated $V_s(t)$ with our measured values. Numerical integration of the DDP system is carried out via nonstandard finite difference scheme, which enforces positivity on electron-hole densities.

[31] T. L. Gilton, J. P. Cowin, G. D. Kubiak, and A. V. Hamza, J. Appl. Phys. **68**, 4802 (1990).